



Cite this: *React. Chem. Eng.*, 2025, 10, 168

## Unveiling the dynamic $\text{CO}_2$ capture performance of $\text{MgO}$ promoted with molten salts and $\text{CaCO}_3$ via fixed bed reactor experiments†

Theodoros Papalas, <sup>ab</sup> Andy N. Antzaras<sup>a</sup> and Angeliki A. Lemonidou <sup>ac</sup>

Carbonate looping using  $\text{MgO}$ -based materials has recently ignited scientific interest for  $\text{CO}_2$  capture at intermediate temperatures (275–375 °C), with the main limitation being the slow carbonation kinetics of  $\text{MgO}$ . Molten alkali nitrates and metal carbonates have been identified as promoters that provide an alternative reaction mechanism for an enhanced carbonation rate. However, the evaluation of the ability of these materials to effectively remove  $\text{CO}_2$  from a gas feed under realistic reactor configurations is still required. This study investigated the  $\text{CO}_2$  capture performance of magnesite-derived  $\text{MgO}$  promoted with limestone and molten Li, Na and K nitrates under carbonate looping conditions in a fixed bed reactor. The  $\text{CO}_2$  capture efficiency was enhanced in the presence of  $\text{H}_2\text{O}$ , by increasing the gas-solid contact time and by decreasing the carbonation temperature. The evaluation demonstrated that ~75%  $\text{CO}_2$  stripping of a gas feed with 30%  $\text{CO}_2$  concentration at 275 °C and a space velocity of 300  $\text{h}^{-1}$  is possible, a performance that highlights and expands the potential and possible applications of  $\text{MgO}$ -based materials.

Received 12th September 2024,  
Accepted 22nd October 2024

DOI: 10.1039/d4re00432a

rsc.li/reaction-engineering

## 1. Introduction

The heavy reliance on fossil fuels to satisfy the global energy requirements has led to a significant increase in  $\text{CO}_2$  emissions and severe environmental problems. The mitigation of emissions can be attained by adopting renewable resources, increasing the efficiency of current energy technologies and implementing  $\text{CO}_2$  capture, utilisation and storage (CCUS).<sup>1,2</sup> Despite the notable progress in renewable energy technologies, their high costs and low maturity, along with the varying availability across regions and the periodic nature of renewable resources, suggest that the global economy will continue to rely on fossil fuels for the foreseeable future. In contrast, CCUS can be applied by retrofitting fossil fuel-dependent energy systems, such as the heavy industry (cement, steel, and chemicals production), which accounts for 20% of industrial emissions.<sup>3</sup> This approach can help carbon-intensive industries meet the requirements of the energy transition period and operate sustainably in the future. Hence, research should aim to find viable CCUS solutions.

Schemes based on reversible gas–solid reactions between  $\text{CO}_2$  and metal oxides, such as carbonate looping, comprise a promising carbon capture technology.  $\text{CO}_2$  is captured *via* the carbonation of the metal oxide, while the formed carbonate is transferred and decomposed to a second reactor operating at higher temperatures, enabling the reuse of the metal oxide for carbonation.  $\text{CaO}$  has been favoured for this technology due to its high  $\text{CO}_2$  capture capacity (17.8 mmol  $\text{CO}_2$  per g) and fast carbonation kinetics at 550–650 °C.<sup>4–6</sup> Such attributes have enabled the pilot-scale investigation of calcium looping, reaching a technology readiness level of 6–7.<sup>7,8</sup> However, harsh decarbonation temperatures ( $\geq 900$  °C) are detrimental to the  $\text{CaO}$  stability and process energy demand, while they make retrofitting of existing industries less flexible, as flue gas is typically available at lower temperatures.<sup>9,10</sup>

$\text{MgO}$  has recently gained interest due to the favourable thermodynamics (Fig. 1) for carbonation (eqn (1)) at intermediate temperatures (275–375 °C). With a high theoretical  $\text{CO}_2$  capture capacity (24.8 mmol  $\text{CO}_2$  per g) and mild decarbonation conditions (400–450 °C),  $\text{MgO}$  presents a sustainable alternative for flexible  $\text{CO}_2$  capture applications.<sup>4,11,12</sup> The main limitation comprises the slow carbonation kinetics, arising from the high lattice energy of  $\text{MgO}$  and the formation of a non-crystalline carbonate layer of 7 Å thickness in contact with  $\text{CO}_2$ ,<sup>13</sup> resulting in an uptake of less than 0.5 mmol  $\text{CO}_2$  per g after 1 h exposure to  $\text{CO}_2$ .<sup>14,15</sup>



<sup>a</sup> Department of Chemical Engineering, Aristotle University of Thessaloniki, University Campus, 54124 Thessaloniki, Greece.

E-mail: alemonidou@cheng.auth.gr

<sup>b</sup> Department of Chemical Engineering and Biotechnology, University of Cambridge, Philippa Fawcett Drive, CB3 0AS Cambridge, UK. E-mail: tp557@cam.ac.uk

<sup>c</sup> Chemical process & Energy Resource Institute, CPERI/CERTH, 57001 Thermi, Thessaloniki, Greece

† Electronic supplementary information (ESI) available. See DOI: <https://doi.org/10.1039/d4re00432a>



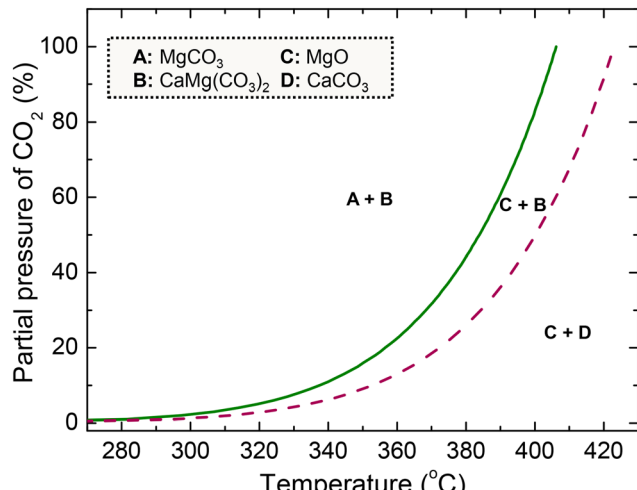


**Fig. 1** Equilibrium curves of the carbonation of pure MgO (solid line) and MgO-CaCO<sub>3</sub> (dashed line) with a CaCO<sub>3</sub> to MgO molar ratio of 0.05 at 1 bar (recreated from ref. 16). In the figure, A refers to MgCO<sub>3</sub>, B to CaMg(CO<sub>3</sub>)<sub>2</sub>, C to MgO and D to CaCO<sub>3</sub>.

Zhang *et al.* proposed adding NaNO<sub>3</sub> as a promoter in MgO, significantly enhancing the CO<sub>2</sub> capture capacity.<sup>17,18</sup> The ability of NaNO<sub>3</sub> to shift to a molten phase under carbonation conditions introduces an alternative reaction mechanism that enables the MgCO<sub>3</sub> nuclei formation and growth. They further noted that the molten alkali salt reduces the energy barrier for the dissociation of MgO to [Mg<sup>2+</sup>⋯O<sup>2-</sup>] ionic pairs. The latter reacts with CO<sub>2</sub> adsorbed on the surface of MgO on the triple phase boundaries, or stated otherwise, the contact points between gas, solid and molten phases, to yield [Mg<sup>2+</sup>⋯CO<sub>3</sub><sup>2-</sup>] ionic pairs that eventually crystallise to MgCO<sub>3</sub>, once the molten phases reach saturation.<sup>18</sup> Dal Pozzo *et al.* also identified the dissolution of MgO to [Mg<sup>2+</sup>⋯O<sup>2-</sup>] ionic pairs as the rate-determining step,<sup>19</sup> while Gao *et al.* found that MgO adsorbs NO<sub>2</sub><sup>+</sup> from the molten phase lowering the barrier of MgO dissolution.<sup>20</sup> Harada *et al.* proposed another carbonation mechanism, suggesting that the molten salt spreads on the surface of MgO and prohibits the formation of non-penetrable carbonate layers. CO<sub>2</sub> dissolved in the molten phase can react with O<sup>2-</sup> available from NaNO<sub>3</sub> to form CO<sub>3</sub><sup>2-</sup> and then with MgO to generate MgCO<sub>3</sub>.<sup>21</sup> Other studies supported this mechanism and proved that MgCO<sub>3</sub> crystallites have a preferred orientation at the interface between MgO and molten NaNO<sub>3</sub>, without excluding triple phase boundaries as the formation point of MgCO<sub>3</sub>.<sup>13,22</sup> Finally, another mechanism proposed by Landuyt *et al.* supports that the MgO surface initially undergoes fast carbonation and the formed carbonates dissolve in [Mg<sup>2+</sup>⋯CO<sub>3</sub><sup>2-</sup>] ionic pairs and then crystallise as MgCO<sub>3</sub>.<sup>23</sup>

Many researchers have also investigated various binary and ternary salt mixtures except for NaNO<sub>3</sub> to evaluate the effect of the composition of the molten phase on the CO<sub>2</sub> capture activity.<sup>19,21,24-26</sup> Addition of alkali nitrates with an alkali of small ionic radius can enhance the CO<sub>2</sub> solubility and thus the CO<sub>2</sub> uptake of the material, while nitrates with an alkali of large ionic radius are resistant to decomposition, thereby retaining

their beneficial effect on multiple carbonation and decarbonation cycles.<sup>12,21</sup> Beyond alkali nitrates, there is high interest in using alkali or alkaline earth carbonate promoters (e.g. Na<sub>2</sub>CO<sub>3</sub>, K<sub>2</sub>CO<sub>3</sub>, CaCO<sub>3</sub>, BaCO<sub>3</sub>) to improve the MgO carbonation rate.<sup>27-30</sup> Carbonates serve as nucleation seeds, which are beneficial due to the autocatalytic behaviour of the nuclei formation and growth mechanism. Moreover, they may also form mixed carbonates with MgO, whose formation is thermodynamically feasible at lower partial pressures of CO<sub>2</sub> compared to MgCO<sub>3</sub>,<sup>13,31,32</sup> as illustrated in Fig. 1 for the case of a mixture of MgO and CaCO<sub>3</sub>. Our previous work examined MgO-based materials derived from magnesite and promoted with limestone and a mixture of Li, Na and K nitrates (Li/Na/K = 30/18/52). Limestone enabled the formation of CaMg(CO<sub>3</sub>)<sub>2</sub> and a fast nucleation rate, when applying a CaCO<sub>3</sub> to MgO molar ratio of 0.05. Increasing the alkali nitrate content accelerated the generation of carbonates, while the optimal molar ratio of alkali nitrates to MgO was equal to 0.20. The optimum CaCO<sub>3</sub> and alkali salt contents resulted in an uptake of 7.2 mmol CO<sub>2</sub> per g (30% CO<sub>2</sub>, 300 °C, 30 min) and minimal activity loss (~6%) after 50 cycles in a thermogravimetric analyser.<sup>16,33</sup>

Despite extensive research on molten salt-promoted MgO, the evaluation of CO<sub>2</sub> capture activity has mainly been conducted with pure CO<sub>2</sub> gas feed and long carbonation durations in thermogravimetric analysers, thereby not reflecting realistic operating conditions. Thermogravimetric analysis can efficiently determine the CO<sub>2</sub> uptake capacity of such materials; however, it is essential to also examine the CO<sub>2</sub> stripping efficiency from the gas feed.<sup>12,34</sup> Chen *et al.* evaluated MgO-based materials promoted with various alkali nitrates and carbonates (LiNO<sub>3</sub>, KNO<sub>3</sub>, Na<sub>2</sub>CO<sub>3</sub>, K<sub>2</sub>CO<sub>3</sub>) in a fixed bed reactor. They found a CO<sub>2</sub> capture efficiency less than 10% when carbonation was conducted at 325 °C even with the use of a gas feed with unrealistically high CO<sub>2</sub> concentration (80% CO<sub>2</sub>) for either pre- or post-combustion CO<sub>2</sub> capture applications.<sup>35</sup> Experiments should be performed under real flow reaction conditions in bench-scale units, with such studies being currently scarce in the literature,<sup>35-40</sup> combined with continuous reactor gas outlet monitoring.

This study builds on our previous work<sup>16,33</sup> and investigates the developed MgO-based material promoted with CaCO<sub>3</sub> and alkali nitrates under carbonate looping conditions *via* fixed bed reactor experiments. The ability to remove CO<sub>2</sub> from a gas feed was evaluated by varying temperature, CO<sub>2</sub> concentration, H<sub>2</sub>O presence and space velocity. The results of this study reveal the potential and limitations of dynamic CO<sub>2</sub> capture at intermediate temperatures and provide insight on the possible industrial applications of the MgO-based materials.

## 2. Materials and methods

### 2.1. Preparation of the material

A MgO-based material was prepared *via* a two-step protocol, initiated by wet mixing of calcined magnesite and calcined limestone in a 12 vol% acetic acid solution and followed by wet impregnation of the resulting solids with Li, Na and K



nitrates (with an atomic ratio of Li/Na/K equal to 30/18/52). The prepared material had nominal molar ratios of  $\text{CaCO}_3$  and alkali salts to  $\text{MgO}$  of 0.05 and 0.20, respectively, and was designated as  $\text{MgCa}_{0.05}\text{A}_{0.20}$ . The detailed preparation protocol and characterisation results, including *ex situ* and *in situ* X-ray diffraction,  $\text{N}_2$  adsorption, and scanning electron microscopy, for both fresh and used materials subjected to carbonate looping conditions can be found elsewhere.<sup>16,33</sup>

## 2.2. Evaluation of the $\text{MgO}$ -based material under carbonate looping conditions

Thermogravimetric analysis (TGA, TG 209 F3 Tarsus, NETZSCH) was utilised to explore the effect of pelletisation on the  $\text{CO}_2$  capture activity of the  $\text{MgCa}_{0.05}\text{A}_{0.20}$  material. After the final calcination step of the preparation protocol at 450 °C, the material powders were compressed into small discs with a manual hydraulic press. The discs were then crushed and sieved to obtain a particle size range of 106 to 212  $\mu\text{m}$ . After loading ~10 mg of the material in an  $\text{Al}_2\text{O}_3$ -based crucible, the temperature was increased to 450 °C under a 100%  $\text{N}_2$  flow to remove any  $\text{CO}_2$  or  $\text{H}_2\text{O}$  captured from the atmosphere. The TGA chamber was cooled down to 300 °C with a rate of 50 °C min<sup>-1</sup> and the gas feed was switched to a 30%  $\text{CO}_2/\text{N}_2$  flow for 30 min to conduct the carbonation stage. Afterwards, the sample was heated up to 450 °C at 10 °C min<sup>-1</sup> to decompose the formed carbonates under a 100%  $\text{N}_2$  flow. A total of 50 carbonation and decarbonation cycles were performed, while the same experiment was conducted also with a non-pelletised material for comparison.

The performance of the  $\text{MgCa}_{0.05}\text{A}_{0.20}$  material was investigated by performing experiments in a continuous flow unit equipped with a fixed bed reactor. A schematic illustration of the unit is available in the ESI† (Fig. S1). The reactor was loaded with 0.5, 2, or 4 g of material with a particle diameter below 106  $\mu\text{m}$  obtained by sieving the material without prior pelletisation. Solids were pre-treated by increasing the temperature to 450 °C under a 100% He flow to release any captured  $\text{CO}_2$  or  $\text{H}_2\text{O}$ . The reactor was then cooled down to 275, 300 or 325 °C and the gas feed was switched to 30%  $\text{CO}_2/\text{He}$  or 15%  $\text{CO}_2/\text{He}$  (50 mL min<sup>-1</sup>) to conduct the carbonation stage. The effect of steam was also examined in an experiment, in which the gas feed passed through a steam saturator to attain a 5%  $\text{H}_2\text{O}$  content. The composition of the carbonation gas feed was selected to replicate the flue gas of the cement industry.<sup>41,42</sup> Carbonation was followed by the increase of temperature at 450 °C and the change of gas feed to 100% He (120 mL min<sup>-1</sup>) to carry out the decarbonation stage. The carbonation and decarbonation stages were repeated for a total of 10 cycles. The duration of the carbonation stage was equal to 30 min, except from the 1st and 10th cycle, where the duration was extended to 60–180 min. The prolonged carbonation stages aimed to fully detect the transition of the kinetically controlled stage to the  $\text{CO}_2$  diffusion through the formed carbonate layers, which was different depending on the remaining operating conditions

(temperature,  $\text{CO}_2$  content in the gas feed, GHSV). On the other hand, decarbonation lasted until the full conversion of carbonates formed in the preceding carbonation stage. In addition to the experiments described, blank experiments were conducted under the same operating conditions with inert  $\text{SiO}_2$  that helped to analyse the results. All experiments were conducted at atmospheric pressure, while pressure drop did not display an increase higher than 15% of inlet pressure, satisfying the general rule of thumb for isobaric conditions at laboratory-scale fixed bed reactor experiments. The detailed methodology followed for analysing the results of TGA and reactor experiments is available in the ESI.†

## 3. Results and discussion

### 3.1. Evaluation of the effect of pelletisation with thermogravimetric analysis

Prior to the fixed bed experiments, the performance of the  $\text{MgCa}_{0.05}\text{A}_{0.20}$  material was investigated in TGA apparatus to check the effect of pelletisation on the performance of the material to be used in the bench-scale unit. The  $\text{MgO}$  carbonation conversion and  $\text{CO}_2$  capture capacity of the material is presented in Fig. 2. The material sieved to obtain a particle size lower than 106  $\mu\text{m}$  without prior pelletisation displayed an initial  $\text{CO}_2$  capture uptake of 7.2 mmol  $\text{CO}_2$  per g of material and a high stability, with a minimal 6% activity loss over 50 consecutive carbonation and decarbonation cycles. On the other hand, the material with a particle size between 106 and 212  $\mu\text{m}$  obtained after pelletisation displayed a ~70% lower initial uptake than the non-pelletised material. However, the material exhibited a continuous self-activation, reaching up to 5.4 mmol  $\text{CO}_2$  per g of material, while the lower initial activity, coupled with the simultaneous self-activation, agrees with previously reported results in the literature for pelletised  $\text{MgO}$ .<sup>35,43</sup>

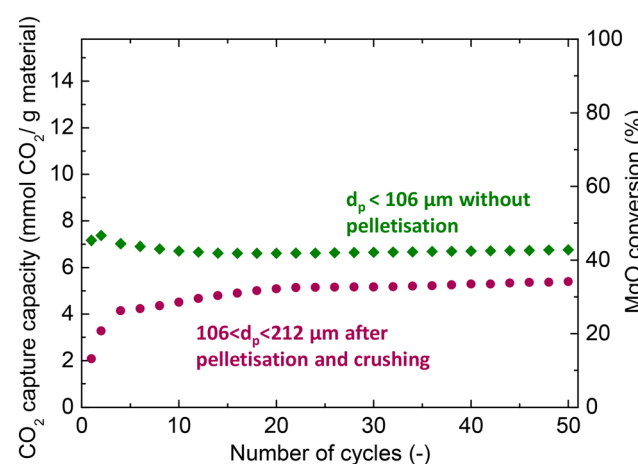


Fig. 2  $\text{CO}_2$  capture efficiency and  $\text{MgO}$  conversion for the  $\text{MgCa}_{0.05}\text{A}_{0.20}$  material obtained with and without pelletisation when investigated via carbonate looping experiments in a thermogravimetric analyser (carbonation stage: 30%  $\text{CO}_2/\text{N}_2$ , 300 °C; decarbonation stage: 450 °C, 100%  $\text{N}_2$ ).



The activity and stability of molten salt-promoted MgO have been linked with various phenomena. While molten salts enhance the CO<sub>2</sub> capture activity, they also dissolve solid components and promote their densification, and thus the annihilation of the pore network, known as liquid phase sintering.<sup>33,44</sup> The cyclic performance is also affected by changes in the distribution of molten salts,<sup>25</sup> as a result of the lower affinity of the molten phase with MgCO<sub>3</sub> compared to MgO.<sup>19,32</sup> The re-distribution can be beneficial for the CO<sub>2</sub> capture activity under certain operating conditions and mask the extent of sintering,<sup>33,45</sup> ultimately being the reason behind the stable performance of the non-pelletised material.

Pelletisation caused a decrease of the surface area (from 10.1 to 5.3 m<sup>2</sup> g<sup>-1</sup>) and pore volume (from 0.08 to 0.03 cm<sup>3</sup> g<sup>-1</sup>), as found by characterising the materials with N<sub>2</sub> adsorption analysis. The inferior textural properties prevent the efficient distribution and exploitation of molten alkali salts, leading to a lower initial CO<sub>2</sub> uptake.<sup>35</sup> However, Rekhtina *et al.* noted that alkali nitrates can gradually decompose and react with CO<sub>2</sub> to form carbonates, which, as mentioned before, act as nucleation seeds and promote carbonation. They further suggested that this effect accounts for the self-activation phenomenon.<sup>31</sup>

In general, granulation of MgO-based CO<sub>2</sub> capture materials is essential for their practical applications. However, current efforts in this area and existing granulation techniques are limited.<sup>38,40,43</sup> Future research should prioritise the development of MgO granules that exhibit strong mechanical properties and high CO<sub>2</sub> capture ability. A key consideration for any granulation method is its scalability for industrial use, since large quantities of MgO are required for practical looping systems. Additionally, the cost-effectiveness of the manufacturing process is another critical factor.<sup>12</sup> In any case, finding an efficient granulation method was rendered out of the scope of this study and thus all experiments described below were performed using a non-pelletised material with a particle size below 106 µm to evaluate the full potential for stripping CO<sub>2</sub> from a gas feedstock.

### 3.2. CO<sub>2</sub> capture and release efficiency in a fixed bed reactor

As described before, evaluating the CO<sub>2</sub> capture capacity with TGA does not provide information on the CO<sub>2</sub> capture efficiency from the gas phase, an important parameter for the application of the proposed MgO-based materials. Thus, this section focuses on the performance evaluation under carbonate looping conditions in a fixed bed reactor. Fig. 3a presents the evolution of the CO<sub>2</sub> concentration over time at the exit of the reactor when loaded either with the reactive MgCa<sub>0.05</sub>A<sub>0.20</sub> or an inert SiO<sub>2</sub> material (blank experiment). The CO<sub>2</sub> signal was initially zero, reflecting the time needed for the flow to reach the analyser and for the latter to respond. In the blank experiment with SiO<sub>2</sub>, the signal gradually increased and stabilised at 30%, the inlet CO<sub>2</sub> concentration. In contrast, the CO<sub>2</sub> signal was noticeably lower in the experiment with MgCa<sub>0.05</sub>A<sub>0.20</sub>, demonstrating the effective CO<sub>2</sub> capture from the gas phase. It was possible to divide the profile into three regimes, as inferred from other studies.<sup>21,35,40,46</sup> There is an initial period (1st regime) that refers to the time needed for MgO, CaCO<sub>3</sub> and CO<sub>2</sub> to be dissolved in the molten salts till saturation and enables the precipitation of the first MgCO<sub>3</sub> and CaMg(CO<sub>3</sub>)<sub>2</sub> nuclei. During this period, CO<sub>2</sub> also reacted with uncoated MgO to form unidentate or bidentate carbonates and this may be the reason behind the extended induction period in the experiment with MgCa<sub>0.05</sub>A<sub>0.20</sub> compared to the inert SiO<sub>2</sub> material, as also stated by Zheng *et al.*<sup>40</sup> After some point, the CO<sub>2</sub> capture performance accelerated (2nd regime), since the molten phase remains oversaturated with dissolved reactants, leading to the gradual growth of the size of the nuclei, a faster step compared to their initial formation and the saturation of the molten phase. After some time, the CO<sub>2</sub> diffusion through the formed carbonate layers becomes the kinetically controlled stage, which is slower compared to the previous stages, leading to the gradual reduction of the attained CO<sub>2</sub> capture over time (3rd regime). From an industrial viewpoint, it is preferred to operate before the 3rd regime, where the CO<sub>2</sub> capture is high.

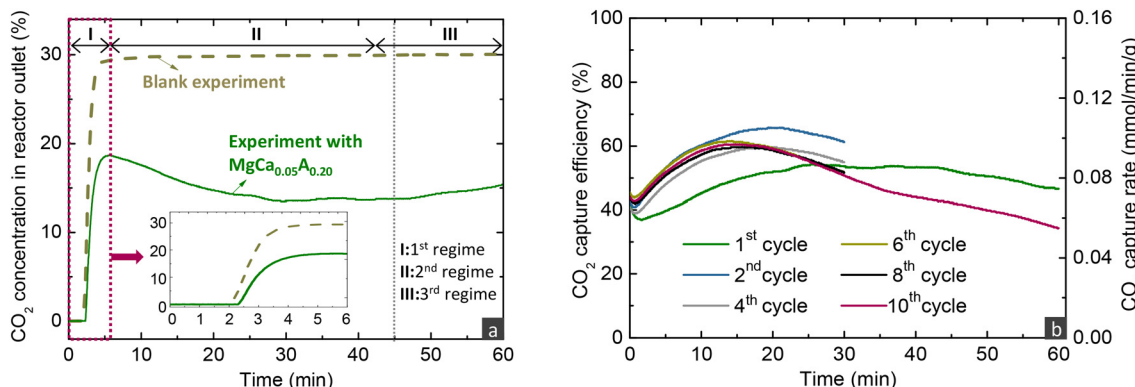


Fig. 3 (a) Outlet CO<sub>2</sub> concentration over time for the blank experiment with SiO<sub>2</sub> and the experiment with the MgCa<sub>0.05</sub>A<sub>0.20</sub> material and (b) CO<sub>2</sub> capture efficiency and rate over time for the MgCa<sub>0.05</sub>A<sub>0.20</sub> material during the carbonation stage of different cycles when investigated via carbonate looping experiments in a fixed bed reactor (carbonation stage: 30% CO<sub>2</sub>/He, 300 °C, 300 h<sup>-1</sup>; decarbonation stage: 450 °C, 100% He, 720 h<sup>-1</sup>). The inset in figure (a) is the magnification for the first 6 min.



The recorded  $\text{CO}_2$  concentration enabled the calculation of the  $\text{CO}_2$  capture efficiency and rate, as described in the methodology in the ESI.† Fig. 3b illustrates the results from the investigation of the  $\text{MgCa}_{0.05}\text{A}_{0.20}$  material in 10 consecutive carbonation and decarbonation cycles in a fixed bed reactor containing 4 g of the material. The first and last cycles featured an extended carbonation duration of 60 minutes, while the intermediate cycles lasted 30 minutes each. For simplicity, the data from the first 4 minutes of exposure to  $\text{CO}_2$  are excluded from the figure. With the exception of the initial cycle, the  $\text{CO}_2$  capture efficiency and rate in the first and second regimes remained consistent throughout the subsequent cycles, attaining a  $\text{CO}_2$  capture efficiency and rate of  $\sim 60\%$  and  $\sim 0.09 \text{ mmol min}^{-1} \text{ g}^{-1}$ , respectively, when exposed to a gas stream with 30%  $\text{CO}_2$  concentration at  $300\text{ }^\circ\text{C}$ . The slightly reduced  $\text{CO}_2$  capture performance in the first cycle indicates a lower initial capture capacity; while in subsequent cycles, the material displayed some self-activation, a phenomenon also noted in the literature.<sup>32,33,44</sup>

Fig. 4a displays the outlet  $\text{CO}_2$  concentration over time during the decarbonation stage conducted under a 100% He flow, while increasing the temperature to  $450\text{ }^\circ\text{C}$ . In realistic applications, decarbonation would occur in a  $\text{CO}_2$  atmosphere to yield a high-purity  $\text{CO}_2$  stream, suitable for sequestration or further use. The performance of the studied material under such conditions was investigated in our previous studies.<sup>16,33</sup> In the current work, the  $\text{CO}_2$  release lasted  $\sim 9$  min for all cycles, with the duration being prolonged only in the 1st and 10th cycle, due to the extended preceding carbonation. In contrast to  $\text{MgO}$  carbonation, decarbonation was very fast, due to the applied temperature ( $450\text{ }^\circ\text{C}$ ), which surpasses the minimum temperatures that thermodynamically allow the full conversion of  $\text{MgCO}_3$  or  $\text{CaMg}(\text{CO}_3)_2$  compounds ( $404$  and  $424\text{ }^\circ\text{C}$  as seen in Fig. 1). This implies an enhanced kinetic driving force, which is defined as the difference between the equilibrium  $\text{CO}_2$  partial pressure and the actual  $\text{CO}_2$  partial pressure ( $P_{\text{CO}_2,\text{eq}} - P_{\text{CO}_2}$ ). Several researchers have mentioned that the molten phase can

have a positive effect on the dissociation of carbonate ions and rapid decarbonation of formed carbonates,<sup>21,24,25</sup> while may also initiate at lower temperatures compared to non-promoted  $\text{MgO}$ .<sup>32,44</sup>

Fig. 4b depicts the  $\text{MgO}$  and  $\text{MgCO}_3/\text{CaMg}(\text{CO}_3)_2$  conversions as determined from the carbonation and decarbonation stages, respectively, following the methodology described in eqn S5 and S6 of the ESI.† Similar carbonation and decarbonation conversions were found, indicating that all the  $\text{CO}_2$  captured in each carbonation stage was completely released in the subsequent decarbonation stage. For cycles with a carbonation duration of 30 min, the  $\text{MgO}$  conversion reached 20%, while the transition to the 3rd regime had taken place before the end of the carbonation stage. The low conversion suggests that applying  $\text{MgO}$ -based materials in a realistic process would require a reactor with high solids inventory to attain efficient  $\text{CO}_2$  capture since after surpassing 20%  $\text{MgO}$  conversion, the slow  $\text{CO}_2$  diffusion controls the reaction rate.

It is important to note that the material displayed high stability over cycles. Even though the solids underwent sintering during cycling operation, as verified by employing X-ray diffraction and by comparing the  $\text{MgO}$  crystal size between fresh and used materials (Fig. S2 and Table S1 in the ESI†), the high stability is, as mentioned before, a result of a possible alkali salt redistribution in the surface of  $\text{MgO}$ .<sup>24,33</sup>

### 3.3. Parametric evaluation for the carbonation stage operation

The effect of the different operating parameters was evaluated by conducting experiments of 10 consecutive carbonation and decarbonation cycles. The figures presented below that illustrate the  $\text{CO}_2$  capture efficiency and rate over time profiles contain two curves for each parameter investigated, referring to the first and last carbonation stages of each experiment. Even though the first and last cycles were run for an extended duration (60–180 min) compared to other cycles (30 min), the  $\text{CO}_2$  capture

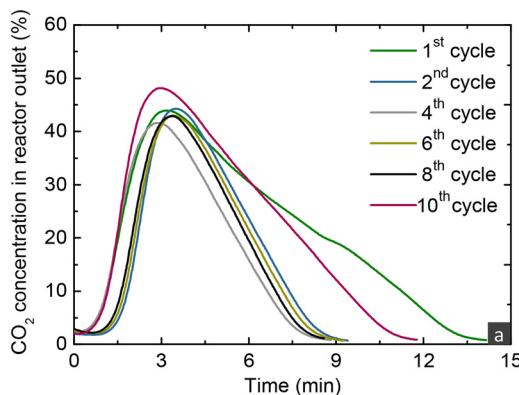
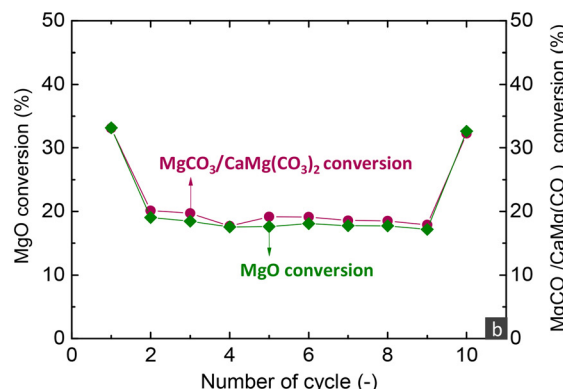


Fig. 4 (a) Outlet  $\text{CO}_2$  concentration during the decarbonation stage of different cycles and (b)  $\text{MgO}$  and  $\text{MgCO}_3/\text{CaMg}(\text{CO}_3)_2$  conversions over cycles for the  $\text{MgCa}_{0.05}\text{A}_{0.20}$  material when investigated via carbonate looping experiments in a fixed bed reactor (carbonation stage: 30%  $\text{CO}_2/\text{He}$ ,  $300\text{ }^\circ\text{C}$ ,  $300 \text{ h}^{-1}$ ; decarbonation stage:  $450\text{ }^\circ\text{C}$ , 100% He,  $720 \text{ h}^{-1}$ ).



capacity as a function of cycles presented below refer to the  $\text{CO}_2$  uptake calculated only from the first 30 min of the carbonation stage.

**3.3.1 Effect of space velocity.** Fig. 5a presents the activity of the  $\text{MgCa}_{0.05}\text{A}_{0.20}$  material with varying GHSVs, attained by altering the solids inventory. The decrease of GHSV, which increased the gas–solid contact time, affected positively the  $\text{CO}_2$  capture efficiency over time, with this effect being more evident when increasing the loading from 0.5 g to 2 g compared to 4 g. The decrease of the  $\text{CO}_2$  concentration in the axial direction of the bed leads to a weak kinetic driving force and inefficient trapping of  $\text{CO}_2$  in the molten phase at the lower reactor sections and thus a non-proportional  $\text{CO}_2$  capture efficiency increase with material loading. This implies that reducing the space velocity to values below 300  $\text{h}^{-1}$  would not greatly enhance the  $\text{CO}_2$  capture efficiency, as also supported by the declining trend of the  $\text{CO}_2$  capture rate (Fig. S3 in the ESI†). Nonetheless, the experiments described below were conducted with a GHSV of 300  $\text{h}^{-1}$ , due to the better stripping efficiency. The duration and volumetric gas flow of the experiments with varying GHSV were maintained the same, ultimately leading to higher  $\text{MgO}$  conversions with a smaller material inventory (Fig. 5b). Despite the different conversion extents, the stability was similar between experiments.

**3.3.2 Effect of  $\text{CO}_2$  concentration and temperature.** Fig. 6 presents the performance of the  $\text{MgCa}_{0.05}\text{A}_{0.20}$  material when investigated at different temperatures (275, 300 and 325 °C) and  $\text{CO}_2$  concentrations (30 and 15%  $\text{CO}_2$ ) during the carbonation stage. The stripping efficiency improved with the increase of  $\text{CO}_2$  concentration and the decrease of temperature. It is remarkable to note that the  $\text{CO}_2$  capture efficiency and rate reached 75% and 0.12  $\text{mmol min}^{-1} \text{g}^{-1}$ , respectively, when conducting the carbonation at 275 °C with the 30%  $\text{CO}_2/\text{He}$  gas feed in all cycles, except for the first one (Fig. 6a). The better performance when operating the carbonation stage at lower temperature can also be derived from the slightly higher  $\text{CO}_2$  capture capacity (Fig. 6b).

Reducing the concentration of  $\text{CO}_2$  to 15%, a condition which simulates realistic operating conditions for post-combustion  $\text{CO}_2$  capture, led to lower  $\text{CO}_2$  capture and  $\text{MgO}$  conversion (Fig. 6c and d), due to the weaker carbonation kinetic driving force. The lower temperature of 275 °C enabled a  $\text{CO}_2$  capture of ~60%, while the transition of the kinetically controlled stage to the  $\text{CO}_2$  diffusion occurred at lower  $\text{MgO}$  conversions than the experiment with a 30%  $\text{CO}_2$  flow.

Temperature has multiple effects on the carbonation mechanism, as discussed in our previous studies,<sup>16,33</sup> while the current results of fixed bed reactor experiments confirm our initial findings. Increasing the temperature contributes beneficially to the Arrhenius parameter of the reaction rate, but is detrimental to the driving force of carbonation due to the decrease of the  $P_{\text{CO}_2,\text{eq}}$  term. Moreover, temperature affects the solubility of all reactants in the molten phase, with the  $\text{CO}_2$  solubility decreasing and the  $\text{MgO}$  and  $\text{CaCO}_3$  solubilities increasing at higher temperatures.<sup>21,47</sup> Nonetheless,  $\text{MgO}$  and  $\text{CaCO}_3$  exhibit different relationships between their solubility and temperature, with the solubility of  $\text{MgO}$  promoted at lower temperatures, while the solubility of  $\text{CaCO}_3$  increases at higher temperatures. Specifically at 275 °C, due to the lower  $\text{CaCO}_3$  solubility, the  $\text{CaMg}(\text{CO}_3)_2$  phase does not crystallise.<sup>16</sup> Thus, at 275 °C,  $\text{CaCO}_3$  contributed to the faster kinetics only by acting as a carbonate seed, promoting the formation of the first nuclei. It is worth to mention that following the transition to the 3rd regime, the  $\text{CO}_2$  capture efficiency decreased faster over time at lower temperatures, due to the lower diffusivity of  $\text{CO}_2$ , a phenomenon also seen in  $\text{CaO}$ -based materials for high-temperature  $\text{CO}_2$  capture.<sup>48</sup>

**3.3.3 Effect of  $\text{H}_2\text{O}$  addition.** All the experiments described above were conducted under dry conditions. However, industrial flue gas contains steam, whose content can reach ~8% in cement production plants or 18–20% in natural gas-fired power plants.<sup>42</sup> The effect of steam addition on the  $\text{CO}_2$  capture capacity of molten salt-promoted  $\text{MgO}$ -based materials has been evaluated *via* TGA experiments,<sup>19,37,49</sup> while in this work, it was examined in the fixed bed reactor (Fig. 7) by

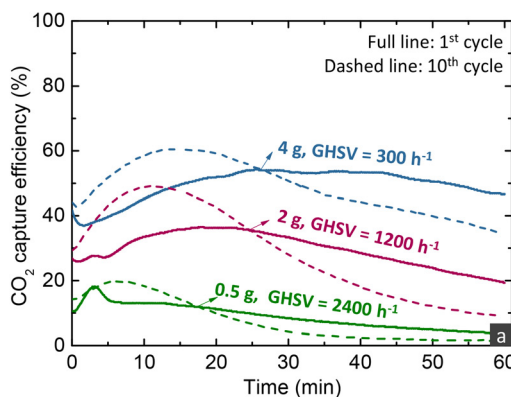
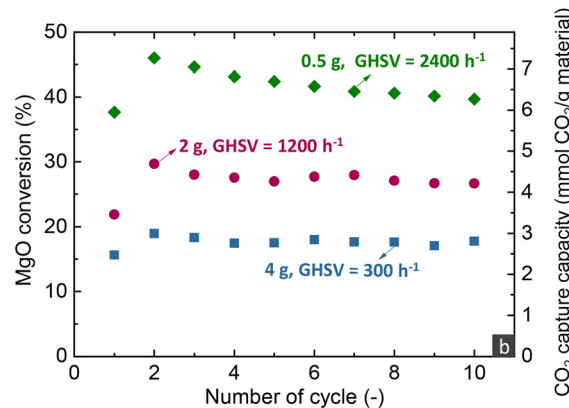


Fig. 5 (a)  $\text{CO}_2$  capture efficiency during the carbonation stage of the 1st and 10th cycles and (b)  $\text{CO}_2$  capture capacity and  $\text{MgO}$  conversion over cycles for the  $\text{MgCa}_{0.05}\text{A}_{0.20}$  material when investigated *via* carbonate looping experiments in a fixed bed reactor with different space velocities for the carbonation stage (carbonation stage: 30%  $\text{CO}_2/\text{He}$ , 300 °C; decarbonation stage: 450 °C, 100% He, 720  $\text{h}^{-1}$ ).



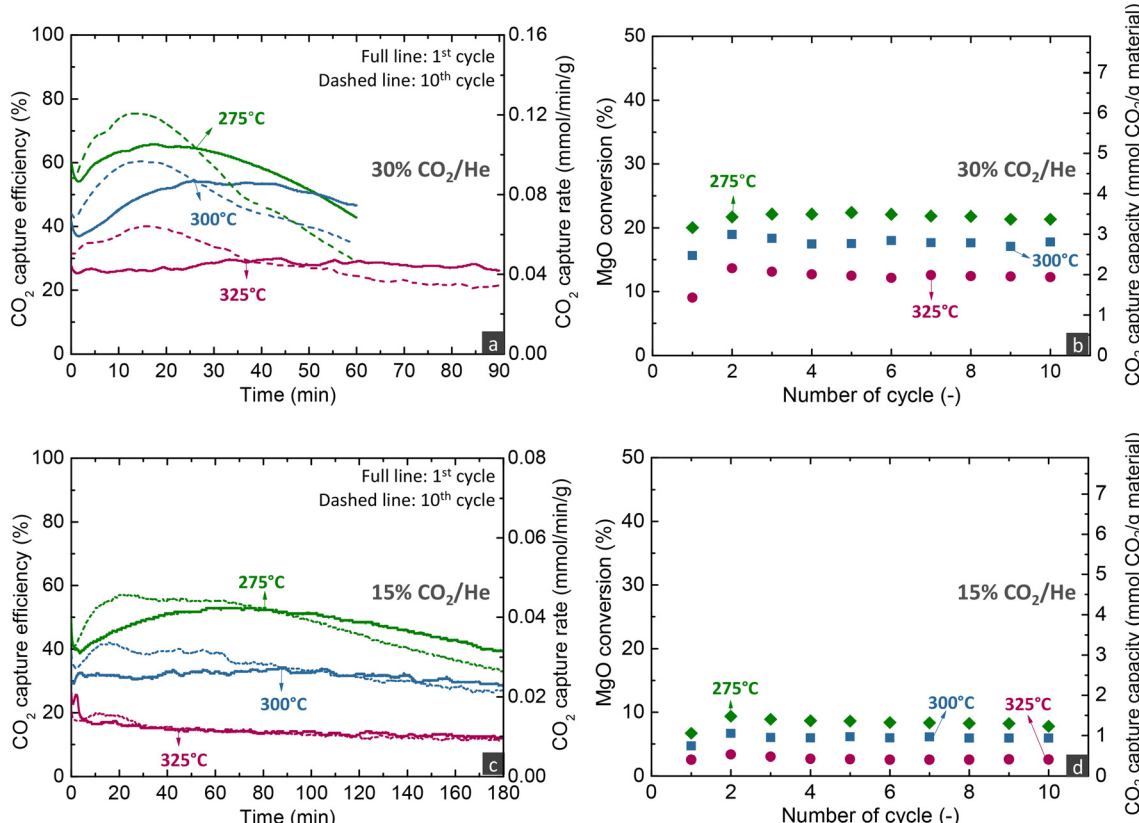


Fig. 6 (a) and (c)  $\text{CO}_2$  capture efficiency and rate during the carbonation stage of the 1st and 10th cycles and (b) and (d)  $\text{CO}_2$  capture capacity and  $\text{MgO}$  conversion over cycles for the  $\text{MgCa}_{0.05}\text{A}_{0.20}$  material when investigated via carbonate looping experiments in a fixed bed reactor with different temperatures and gas feeds for the carbonation stage (carbonation stage:  $300 \text{ h}^{-1}$ ; decarbonation stage:  $450 \text{ }^\circ\text{C}$ , 100% He,  $720 \text{ h}^{-1}$ ).

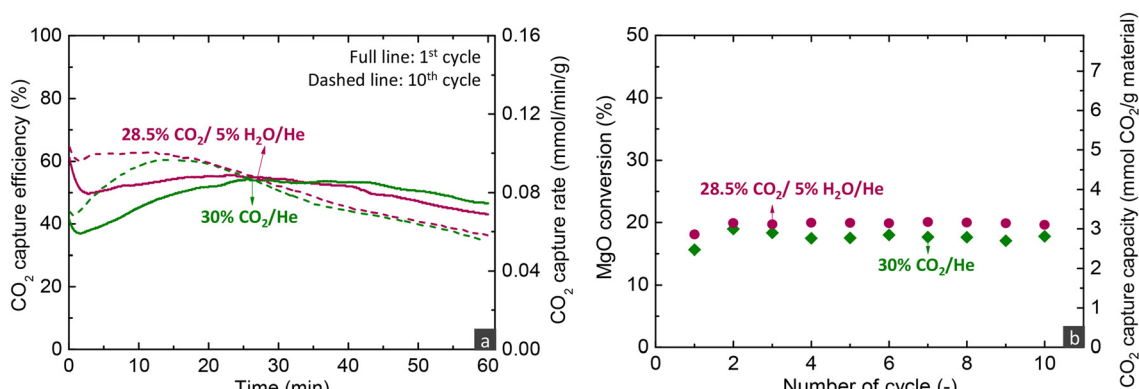


Fig. 7 (a)  $\text{CO}_2$  capture efficiency and rate during the carbonation stage of the 1st and 10th cycles and (b)  $\text{CO}_2$  capture capacity and  $\text{MgO}$  conversion over cycles for the  $\text{MgCa}_{0.05}\text{A}_{0.20}$  material when investigated via carbonate looping experiments in a fixed bed reactor under dry and wet operating conditions for the carbonation stage (carbonation stage:  $300 \text{ h}^{-1}$ ; decarbonation stage:  $450 \text{ }^\circ\text{C}$ , 100% He,  $720 \text{ h}^{-1}$ ).

applying a gas feed with 5%  $\text{H}_2\text{O}$  content. The latter was attained by passing the dry gas feed of 30%  $\text{CO}_2/\text{He}$  through a steam saturator heated at  $33 \text{ }^\circ\text{C}$ , leading to a wet gas feed composed of 28.5%  $\text{CO}_2/5\%$   $\text{H}_2\text{O}/\text{He}$ . The main difference between the dry and wet operating conditions is the slightly higher and more stable  $\text{CO}_2$  capture over time at the beginning of the carbonation stage under the latter conditions, while the  $\text{CO}_2$  capture capacity and cyclic stability were not heavily

affected. The addition of steam in the gas feed of the carbonation stage of  $\text{MgO}$ -based materials has been reported to be beneficial for the  $\text{CO}_2$  capture efficiency. More specifically, the presence of steam results in the formation of intermediate products, such as  $\text{MgO}$  with chemisorbed  $\text{H}_2\text{O}$  ( $\text{MgO}\text{-H}_2\text{O}$ ) or magnesium hydroxide ( $\text{Mg}(\text{OH})_2$ ), which enable the relaxation of the chemical bonds of the  $\text{MgO}$  lattice, the interaction with  $\text{CO}_2$  and initial  $\text{CO}_2$  capture. The decomposition of these

components can also reconstruct the pores, which facilitates the diffusion of gas components and promotes the CO<sub>2</sub> capture.<sup>37,50</sup> This work supports that the presence of steam can have a positive effect on the CO<sub>2</sub> capture efficiency and rate.

Overall, the parametric analysis on the carbonation stage revealed that the MgCa<sub>0.05</sub>A<sub>0.20</sub> material can attain 75% CO<sub>2</sub> capture efficiency from a gas feed with 30% CO<sub>2</sub> at a significantly low temperature of 275 °C, for low MgO conversions (<20%) in the kinetically controlled regime. However, this result was observed with a quite low space velocity (300 h<sup>-1</sup>), a performance which contrasts sharply the behaviour of CaO-based materials used for CO<sub>2</sub> capture at high temperatures (600–750 °C). Our previous studies demonstrated that such materials can attain ~90% capture from a gas feed with 12% CO<sub>2</sub> at 650 °C, while the transition of the kinetically controlled stage to the slow CO<sub>2</sub> diffusions occurs after reaching 70% CaO conversion.<sup>5,6</sup> Moreover, the CaO-based materials attained this activity in shorter contact times (GHSV > 5000 h<sup>-1</sup>) than MgO-based materials (300 h<sup>-1</sup>).

Even though these discrepancies can be attributed to the different reaction mechanisms of the two materials and the faster carbonation kinetics of CaO mostly because of the higher temperature used, they highlight that CaO-based materials exhibit better CO<sub>2</sub> stripping efficiency compared to MgO-based materials, which indicates that the former materials are perhaps more suitable for post-combustion CO<sub>2</sub> capture applications. However, the promising activity of MgO-based materials and their ability to react with CO<sub>2</sub> at intermediate temperatures merit further investigation, particularly in higher operating pressure applications and the intensification of H<sub>2</sub>-producing technologies operating at similar temperatures to MgO, such as sorption-enhanced water gas shift and steam reforming of methanol.<sup>51,52</sup>

## 4. Conclusions

MgO has emerged as a promising material for CO<sub>2</sub> capture at intermediate temperatures (275–375 °C). However, its broad application has been limited by its slow carbonation kinetics. Recent research has focused on developing MgO-based materials promoted with alkali salts, which enhance the carbonation kinetics *via* an alternative reaction mechanism. Despite extensive evaluations of the CO<sub>2</sub> capture activity of these materials with thermogravimetry, there has been a lack of consideration for the efficiency of stripping CO<sub>2</sub> from a gas feedstock in realistic reactor configurations. In this work, we evaluated a mineral MgO-based material promoted with limestone and Li/Na/K nitrates with molar ratios of CaCO<sub>3</sub> and alkali salts to MgO equal to 0.05 and 0.20, respectively, by conducting carbonate looping experiments in a fixed bed reactor. The results showed that carbonation initiates with a high CO<sub>2</sub> capture efficiency and rate, followed by a gradual decrease of performance due to the slow diffusion of CO<sub>2</sub> through the formed carbonate products. The transition between the fast and slow carbonation was found to occur at very low MgO conversions (<20%), dependent on the CO<sub>2</sub> content of the

gas feed. The parametric analysis for the carbonation stage revealed that lowering the operating temperature to 275 °C enables ~75% and ~60% CO<sub>2</sub> stripping efficiency from a 30% and 15% CO<sub>2</sub> feed, respectively, while the increase of space velocity and the presence of H<sub>2</sub>O promote the carbonation rate. Overall, even though the activity of MgO-based materials for post-combustion CO<sub>2</sub> capture may be inferior to CaO-based materials, the results of this study highlight the potential of MgO-based materials for CO<sub>2</sub> capture and process intensification purposes.

## Data availability

The data supporting this article have been included as part of the ESI.†

## Author contributions

Theodoros Papalas: conceptualisation, formal analysis, investigation, methodology, validation, visualisation, and writing – original draft. Andy N. Antzaras: validation, supervision, and writing – review & editing. Angeliki A. Lemonidou: supervision, writing – review & editing, resources, project administration, and funding acquisition.

## Conflicts of interest

There are no conflicts to declare.

## Acknowledgements

This research has been co-financed by the European Regional Development Fund of the European Union and Greek national funds through the Operational Program Competitiveness, Entrepreneurship and Innovation, under the call RESEARCH – CREATE – INNOVATE (project code: T1EDK-01532).

## References

1. S. Fawzy, A. I. Osman, J. Doran and D. W. Rooney, *Environ. Chem. Lett.*, 2020, **18**, 2069–2094.
2. IEA, Net zero by 2050: A roadmap for the global energy sector, 2021.
3. IEA, Energy Technology Perspectives 2020 – Special Report on Carbon Capture Utilisation and Storage, 2020.
4. M. T. Dunstan, F. Donat, A. H. Bork, C. P. Grey and C. R. Müller, *Chem. Rev.*, 2021, **121**, 12681–12745.
5. T. Papalas, A. N. Antzaras and A. A. Lemonidou, *Ind. Eng. Chem. Res.*, 2020, **59**, 9926–9938.
6. A. N. Antzara, A. Arregi, E. Heracleous and A. A. Lemonidou, *Chem. Eng. J.*, 2018, **333**, 697–711.
7. J. A. Garcia, M. Villen-Guzman, J. M. Rodriguez-Maroto and J. M. Paz-Garcia, *J. Environ. Chem. Eng.*, 2022, **10**, 108470.
8. S. A. Theofanidis, A. N. Antzaras and A. A. Lemonidou, *Curr. Opin. Chem. Eng.*, 2023, **39**, 1–10.
9. R. Han, Y. Wang, S. Xing, C. Pang, Y. Hao, C. Song and Q. Liu, *Chem. Eng. J.*, 2022, **450**, 137952.



10 J. Chen, L. Duan and Z. Sun, *Energy Fuels*, 2020, **34**, 7806–7836.

11 A. H. Ruhaimi, M. A. A. Aziz and A. A. Jalil, *J. CO<sub>2</sub> Util.*, 2020, **43**, 101357.

12 Y. Hu, Y. Guo, J. Sun, H. Li and W. Liu, *J. Mater. Chem. A*, 2019, **7**, 20103–20120.

13 A. H. Bork, M. Rekhtina, E. Willinger, P. Castro-Fernández, J. Drnec, P. M. Abdala and C. R. Müller, *Proc. Natl. Acad. Sci. U. S. A.*, 2021, **118**, e2103971118.

14 K. K. Han, Y. Zhou, W. G. Lin and J. H. Zhu, *Microporous Mesoporous Mater.*, 2013, **169**, 112–119.

15 M. Bhagiyalakshmi, J. Y. Lee and H. T. Jang, *Int. J. Greenhouse Gas Control*, 2010, **4**, 51–56.

16 T. Papalas, I. Polychronidis, A. N. Antzaras and A. A. Lemonidou, *J. CO<sub>2</sub> Util.*, 2021, **50**, 101605.

17 K. Zhang, X. S. Li, Y. Duan, D. L. King, P. Singh and L. Li, *Int. J. Greenhouse Gas Control*, 2013, **12**, 351–358.

18 K. Zhang, X. S. Li, W. Z. Li, A. Rohatgi, Y. Duan, P. Singh, L. Li and D. L. King, *Adv. Mater. Interfaces*, 2014, **1**, 1400030.

19 A. Dal Pozzo, A. Armutlulu, M. Rekhtina, P. M. Abdala and C. R. Müller, *ACS Appl. Energy Mater.*, 2019, **2**, 1295–1307.

20 W. Gao, J. Xiao, Q. Wang, S. Li, M. A. Vasiliades, L. Huang, Y. Gao, Q. Jiang, Y. Niu, B. Zhang, Y. Liu, H. He and A. M. Efsthathiou, *Adv. Mater.*, 2021, **34**, 2106677.

21 T. Harada, F. Simeon, E. Z. Hamad and T. A. Hatton, *Chem. Mater.*, 2015, **27**, 1943–1949.

22 H. A. Lara-García, W. Gao, A. Gómez-Cortés, G. Diaz, H. Pfeiffer and Q. Wang, *Ind. Eng. Chem. Res.*, 2019, **58**, 5501–5509.

23 A. Landuyt, P. V. Kumar, J. A. Yuwono, A. H. Bork, F. Donat, P. M. Abdala and C. R. Müller, *JACS Au*, 2022, **2**, 2731–2741.

24 H. Jeon, M. L. T. Triviño, S. Hwang, J. H. Moon, J. Yoo and J. G. Seo, *J. CO<sub>2</sub> Util.*, 2020, **39**, 101153.

25 H. Lee, M. L. T. Trivinò, S. Hwang, S. H. Kwon, S. G. Lee, J. H. Moon, J. Yoo and J. G. Seo, *ACS Appl. Mater. Interfaces*, 2018, **10**, 2414–2422.

26 X. Zhao, G. Ji, W. Liu, X. He, E. J. Anthony and M. Zhao, *Chem. Eng. J.*, 2018, **332**, 216–226.

27 A. T. Vu, K. Ho, S. Jin and C. H. Lee, *Chem. Eng. J.*, 2016, **291**, 161–173.

28 H. Cui, Q. Zhang, Y. Hu, C. Peng, X. Fang, Z. Cheng, V. V. Galvita and Z. Zhou, *ACS Appl. Mater. Interfaces*, 2018, **10**, 20611–20620.

29 H. Cui, Z. Cheng and Z. Zhou, *J. Mater. Chem. A*, 2020, **8**, 18280–18291.

30 L. Wang, Z. Zhou, Y. Hu, Z. Cheng and X. Fang, *Ind. Eng. Chem. Res.*, 2017, **56**, 5802–5812.

31 M. Rekhtina, M. Krödel, Y. H. Wu, A. Kierzkowska, F. Donat, P. M. Abdala and C. R. Müller, *Sci. Adv.*, 2023, **9**, eadg5690.

32 S. I. Jo, Y. I. An, K. Y. Kim, S. Y. Choi, J. S. Kwak, K. R. Oh and Y. U. Kwon, *Phys. Chem. Chem. Phys.*, 2017, **17**, 6224–6232.

33 T. Papalas, A. N. Antzaras and A. A. Lemonidou, *J. CO<sub>2</sub> Util.*, 2021, **53**, 101725.

34 F. Donat and C. R. Müller, *Curr. Opin. Green Sustainable Chem.*, 2022, **36**, 100645.

35 J. Chen, L. Duan, F. Donat and C. R. Müller, *ACS Sustainable Chem. Eng.*, 2021, **9**, 6659–6672.

36 P. Teixeira, P. Correia and C. I. C. Pinheiro, *Chem. Eng. Sci.*, 2024, **289**, 119856.

37 G. Bang, K.-M. Kim, S. Jin and C.-H. Lee, *Chem. Eng. J.*, 2022, **433**, 134607.

38 Y. Cai, W. Liu, Z. Sun, Y. Yang and P. Li, *J. CO<sub>2</sub> Util.*, 2022, **61**, 102047.

39 K. H. Chai, L. K. Leong, S. Sethupathi, K. C. Chong, T. C. K. Yang, S. P. Ong and Y. H. Yap, *Chem. Eng. J. Adv.*, 2024, **17**, 100578.

40 Y. Zheng, J. Wu, L. Zhang, Y. Guo, Z. Xu, Y. Huang, P. Huang, J. Zhang and C. Zhao, *Chem. Eng. J.*, 2022, **450**, 137944.

41 A. Samanta, A. Zhao, G. K. H. Shimizu, P. Sarkar and R. Gupta, *Ind. Eng. Chem. Res.*, 2012, **51**, 1438–1463.

42 D. Ipsakis, G. Varvoutis, A. Lampropoulos, S. Papaefthimiou, G. E. Marnellos and M. Konsolakis, *Renewable Energy*, 2021, **179**, 1884–1896.

43 Y. Hu, X. Liu, Z. Zhou, W. Liu and M. Xu, *Fuel*, 2017, **187**, 328–337.

44 S. Jin, K. Ho, A. T. Vu and C. H. Lee, *Energy Fuels*, 2017, **31**, 9725–9735.

45 X. Ma, H. Cui, Z. Cheng and Z. Zhou, *AIChE J.*, 2023, **69**, e18146.

46 W. Gao, M. A. Vasiliades, C. M. Damaskinos, M. Zhao, W. Fan, Q. Wang, T. R. Reina and A. M. Efsthathiou, *Environ. Sci. Technol.*, 2021, **55**, 4513–4521.

47 T. Harada and T. A. Hatton, *Chem. Mater.*, 2015, **27**, 8153–8161.

48 Y. A. Criado, B. Arias and J. C. Abanades, *Ind. Eng. Chem. Res.*, 2018, **57**, 12595–12599.

49 S. Jin, K. Ho and C. H. Lee, *Chem. Eng. J.*, 2018, **333**, 697–711.

50 W. Gao, L. Sun and Q. Wang, in *Pre-combustion Carbon Dioxide Capture Materials*, ed. Q. Wang, Royal Society of Chemistry, 2018, pp. 61–143.

51 Y. Hu, H. Cui, Z. Cheng and Z. Zhou, *Chem. Eng. J.*, 2018, **377**, 119823.

52 H. Li, H. Tian, S. Chen, Z. Sun, T. Liu, R. Liu, S. Assabumrungrat, J. Saupsor, R. Mu, C. Pei and J. Gong, *Appl. Catal., B*, 2020, **276**, 119052.

